NOx decomposition using Ni- and Fe-loaded biocarbon catalysts

Théodore Graul, María González Martínez, Yi Qiu, Floriane Fourgeaud, Kuo Zeng, Ange Nzihou

194 (2024) 206982

Contents lists available at ScienceDirect

Applied Catalysis O: Open

journal homepage: www.elsevier.com/locate/apcato

NO_x decomposition using Ni- and Fe-loaded biocarbon catalysts

Théodore Graul [a], María González Martínez [a], Yi Qiu [a,b], Floriane Fourgeaud [a], Kuo Zeng [b], Ange Nzihou [a,*]

[a] Université de Toulouse, Mines Albi, UMR CNRS 5302, Centre RAPSODEE, Campus Jarlard, Route de Teillet, 81000 Albi, France
[b] State Key Laboratory of Coal Combustion, Huazhong University of Science and Technology, 1037 Luoyu Road, Wuhan, Hubei 430074, China

ARTICLE INFO

Keywords:
Biocarbon
Catalyst
NO decomposition
Nickel
Iron

ABSTRACT

Fern and willow (W) impregnated with heavy metals (Ni/Fe) were pyrolyzed (800 °C, N_2) to produce heavy metal-loaded biocarbon to catalyze NO decomposition ($deNO_x$). The effects of reaction temperature (200, 350 and 500 °C), biomass type and impregnated metals on $deNO_x$ performance were investigated. WFe and WNi achieved the highest $deNO_x$ performance at 200 °C (16.5%) and 500 °C (30.6%) respectively. The biocarbon composition and structure were crucial for NO adsorption and metal dispersion, which induced higher CO_2 adsorption (TPO), high specific surface area (419.1 m^2/g for WNi), and highly dispersed small Ni particles (SEM). The main routes for $deNO_x$ evidenced by on-line monitoring were direct decomposition of NO into N_2 and O_2, and NO reduction to N_2, CO and CO_2 by biocarbon sites. Dispersed catalytic metals, as well as NO adsorption and reactivity by biocarbon functional groups, reflect the cost-effective and eco-friendly $deNO_x$ potential of biocarbon catalysts.

1. Introduction

As one of the major air pollutants, nitrogen oxides (NO_x) are responsible to the formation of acid rain, photochemical smog, the depletion of ozone and respiratory diseases, seriously affecting human health and the environment [1–3]. NO_x and mainly nitrogen oxide (NO, > 95% emissions) are mostly emitted from fossil fuel combustion and fundamental industrial processes [4,5]. Currently, selective catalytic reduction (SCR) and three-way catalysts are widely used to decompose NO_x in fixed and mobile sources, respectively [6–8].

The homogeneous decomposition of NO (**Eq**.1) is thermodynamically feasible with $\Delta G = -86.6\ kJ/mol$ at 100 °C [2]. However, the strong binding energy between N and O atom (~ 630.6 kJ/mol) results in a high activation energy (~335 kJ/mol) for this reaction [9].

$$NO \rightarrow \frac{1}{2} N_2 + \frac{1}{2} O_2 \quad \textbf{(1)}$$

The N—O binding energy complicates activation on catalytic surfaces [10,11]. Therefore, the catalytic pathways for NO direct decomposition remain controversial with various mechanisms being proposed [2], including the Langmuir–Hinshelwood model (**Eq**.2–5, * for vacant active sites) where reactive species react on the catalyst surface [12,13].

Another is the Eley-Rideal (**Eq**.6–10) model where reactive species adsorbed on the surface react with others in the medium surrounding the catalyst [13,14].

$$2[NO + * \longleftrightarrow NO^*] \quad \textbf{(2)}$$

$$2NO^* \longrightarrow N_2O^* + O^* \ (Rate\ Determining\ Step, RDS) \quad \textbf{(3)}$$

$$N_2O^* \longrightarrow N_2 + O^* \quad \textbf{(4)}$$

$$2O^* \longleftrightarrow O_2 + 2^* \quad \textbf{(5)}$$

$$NO + {}^* \longleftrightarrow NO^* \quad \textbf{(6)}$$

$$NO + NO^* \longrightarrow N_2O_2^* \ (RDS) \quad \textbf{(7)}$$

$$N_2O_2^* + {}^* \longrightarrow N_2O^* + O^* \quad \textbf{(8)}$$

$$N_2O^* \longrightarrow N_2 + O^* \quad \textbf{(9)}$$

$$2O^* \longleftrightarrow O_2 + 2^* \quad \textbf{(10)}$$

Noble metals [15–18], simple metal oxides [19–22], rare-earth metal

* Corresponding author at: Université de Toulouse, Mines Albi, UMR CNRS 5302, Centre RAPSODEE, Campus Jarlard, Route de Teillet, 81000 Albi, France.
E-mail addresses: theodore.graul@mines-albi.fr (T. Graul), maria.gonzalez_martinez@mines-albi.fr (M. González Martínez), yi.qiu@mines-albi.fr (Y. Qiu), floriane.fourgeaud@mines-albi.fr (F. Fourgeaud), zengkuo666@hust.edu.cn (K. Zeng), ange.nzihou@mines-albi.fr (A. Nzihou).

https://doi.org/10.1016/j.apcato.2024.206982
Received 24 April 2024; Received in revised form 9 July 2024; Accepted 16 July 2024
Available online 17 July 2024

oxides [13,23,24], complex metal oxides [25–27] to zeolites [28–30] and graphene catalysts [13,31] can bring down the NO activation energy. These catalysts however suffer high prices from solvent and energy-intensive processes, high reaction temperatures and low oxygen-related activity that could impede their use and the environment [2,32]. Therefore, there is an urgent need to develop catalysts that decompose NO_x pollutants effectively, economically and sustainably. Transition metals generally have strong redox ability because of their unique valence electron structure [8,33,34]. Among them, iron (Fe) and nickel (Ni) are widely available, cheap and not toxic (Fe). Above 200 °C, the addition of both Ni and Fe on carbon surface significantly enhanced $deNO_x$, with Ni generally outperforming Fe [35]. The combined effect of both metals has only been recently studied, with improved NO_x adsorption and reaction by the complementary behavior of the two active sites [36].

Biocarbon (or biochar) is an eco-friendly carbon-rich material produced through biomass thermal conversion, which has been given diverse applications including catalytic supports and catalysts [37–40]. Biocarbon has been found effective in $deNO_x$ without the use of additional reducing agents such as ammonia [41,42]. This has been linked to intrinsic heteroatoms (e.g. N, O, S, P) and biocarbon inherent or impregnated metallic compounds [18,37]. Impregnation incorporates active metallic species into the biocarbon structure and imitates plants that enrich themselves with heavy metals during their growth [43–45]. Active interfaces and binding sites are created during impregnation, resulting in higher active surface area and total pore volume [46]. NO will preferentially react with zerovalent Ni and Fe impregnated on biocarbon, and form N_2 or N_2O. The resulting metal oxides are then reduced by carbon, forming zerovalent metals again (**Eq**.11–13, with M = Ni or Fe, and x = 1 or 2).

$$M + {}^{*} \longrightarrow M^{*} \quad \textbf{(11)}$$

$$2M^{*} + 2NO \longrightarrow 2MO^{*} + N_2 \quad \textbf{(12)}$$

$$xMO^{*} + C \longrightarrow xM^{*} + CO_x \quad \textbf{(13)}$$

In this study, fern and willow impregnated with Ni and Fe before pyrolysis were used to mimic an easily available hyperaccumulative bioresource with short growth cycle [45,47,48]. Biocarbon catalysts were characterized before and after $deNO_x$ experiments in terms of elemental and inorganic composition, specific surface area, surface functional groups, porosity, and thermal stability. The effects of reaction temperature, nature of biomass and impregnated metals, linked to the biocarbon catalyst properties, on $deNO_x$ performance were investigated.

2. Materials and methods

2.1. Preparation of biocarbon catalysts

Fern (F) and willow (W) were selected as raw materials for this study. As short rotation coppices, they present a fast growth and short cycle, which justified their interest in phytoremediation and rapid metal accumulation. For the large-scale production of biocarbon catalysts, availability and abundance of the bioresource in the territory needs to be considered for its selection. To simulate heavy metal content, impregnation of raw biomass with Ni and Fe nitrates ($Ni(NO_3)_2$, $Fe(NO_3)_3$) was carried out.

Wetness impregnation (WI) was applied to raw biomass. This method consists of the active metallic species incorporation into biocarbon structures via (in-situ) mixing of feedstock with metal precursors, forming active interfaces and binding sites [46,49]. For each round of impregnation, 20 g of biomass was submerged in 1 L aqueous solutions containing Fe or Ni nitrates, stirred for 3 days to reach optimal dispersion of metallic species [50]. The amount of Fe and Ni nitrates used are calculated based on the final goal of reaching a same quality of metal load in biocarbon (3 wt.% in biocarbon). Three different Fe and Ni impregnation concentrations were used for fern (FFe*, FNi* and FNiFe were only tested at 500 °C). Following the impregnation, the biomass was filtered and dried for 24 h at 60 °C [50]. The impregnated biomass was pyrolyzed under 1 L/min N_2 from 25 to 800 °C, at 2 °C/min, followed by a 1 h-isothermal step at 800 °C. For each pyrolysis experiment, 9–10 g of biomass was placed into the crucible and the biocarbon generated was 2–3 g depending on the sample. This would give a proximate solid yield of 25 wt.%. Unimpregnated fern biocarbon (RF) and willow biocarbon (RW) were prepared under the same pyrolysis conditions for comparison.

2.2. $DeNO_x$ experiments

The performance of prepared biocarbon catalysts in $deNO_x$ was tested at laboratory scale. The experimental set-up (Fig. 1) consisted in a fixed-bed reactor followed by a cold trap system, an on-line **µ**GC (Agilent 990) and an on-line NO_x analyzer (ThermoScientific, 42i-HL). The fixed-bed reactor consisted of a quartz tube with a porous disc in the isothermal area of the reactor, so the sample could be placed in a quartz crucible on it. The fixed-bed reactor was arranged vertically in a Heraeus furnace (D-6450 Hanau), able to work up to 1100 °C. Cold traps were used to trap impurities and moisture that may end up in the circuit. The first cold trap, filled with isopropanol and cooled by a thermostatic bath, was used to trap soot and tars that can form during treatments at high temperatures (500 °C). The other two traps, at room temperature, respectively filled with silica gel and empty, were used to trap residual moisture to prevent damage to the analytical devices. On-line **µ**GC monitored the outlet gas composition (N_2, O_2, CO_2, CO and H_2) with an interval of 2.5 min. On-line NO_x analyzer monitored outlet NO and NO_2 concentration with an averaging time of 1 min.

4 g (i.e. a bed height of around 2 cm) of biocarbon catalyst were placed in a quartz crucible inside the quartz reactor [51]. The temperature of the oven was then raised to 140 °C under constant argon (Ar) flow (300 mL/min, 1 atm) and kept for 15 min to eliminate traces of moisture and undesirable compounds [52–54]. After that, the temperature was raised to the experiment temperature (200, 350 or 500 °C) with a heating rate of 10 °C/min. The beginning of the experiment was considered when the isothermal step reached the experiment temperature (set as $t = 0$ min, Fig. 2). During the first 30 min, CO, CO_2 and H_2 were released from the biocarbon. The production was related to the thermal decomposition of the catalysts and was measured by the online **µ**GC under Ar flow. At 30 min, the inlet gas was switched to a constant flow of 1021 ppm NO in Ar (300 mL/min, 1 atm). This concentration was chosen to simulate the high concentration of nitric oxide (600–1200 ppm) in exhaust gas [10,42]. The $deNO_x$ performance was tested for 1 h. Finally, the gas was switched again to Ar and kept for 30 min to observe the desorption phase. At the end of the experiment, the reactor was cooled down and the spent biocarbon catalyst was stored for characterization. Extended experiments were carried out for selected samples to evaluate the degradation of catalysts, with a longer exposure under NO flow (4 h).

To compare the $deNO_x$ performance, the $deNO_x$ ratio (X_{NO}) was calculated as the percentage of NO being removed after contact with biocarbon catalysts (**Eq**.14).

$$X_{NO} = \frac{C_{NO,in} - C_{NO,out}}{C_{NO,in}} \quad \textbf{(14)}$$

Where X_{NO} is the $deNO_x$ ratio, $C_{NO,in}$ is the inlet NO concentration, $C_{NO,out}$ is the outlet NO concentration, which is the measured value on the NO_x analyzer. For $C_{NO,in}$, it is calculated with the average NO concentration of respective blank test.

Repetitions of experiments were conducted and resulted in a relative standard deviation (RSD) of X_{NO} (**Eq**.14) inferior to 2%.

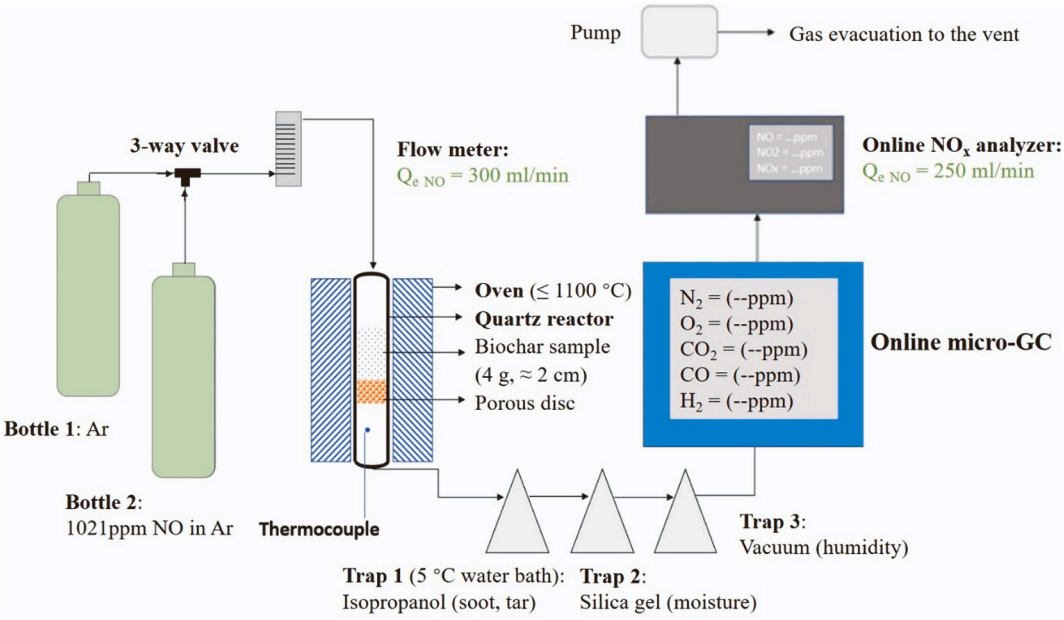

Fig. 1. Experiment set-up for testing deNO$_x$ performance of biocarbon catalysts.

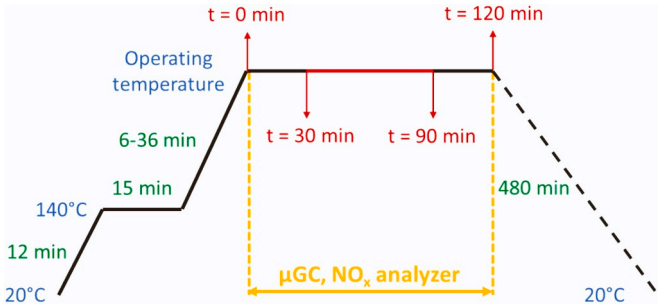

Fig. 2. Temperature program of the oven during one standard experiment.

2.3. Characterization of biocarbon catalysts

The organic element content (carbon, hydrogen, nitrogen, sulfur, CHNS) and inorganic element content were determined using the elemental analyzer Flash 2000 and induced-coupled plasmas atomic emission spectroscopy (ICP-AES) Ultima 2, before and after deNO$_x$ experiments. The dispersion of metals on the carbonaceous matrix were investigated with scanning electron microscopy (SEM). The biocarbon thermal stability and ash content were determined with thermogravimetric analysis coupled with differential scanning calorimetry (TGA-DSC, Seteram Labsys Evo 1600). The surface area and surface chemical groups were characterized by N_2 adsorption using Brunauer-Emmett-Teller calculations (BET, Micromeritics Tristar II 3020) and temperature programmed desorption, reduction and oxidation (TPD, TPR, TPO, Micromeritics Autochem 2920), respectively.

3. Results and discussion

3.1. Biocarbon characterization

3.1.1. Elemental composition

The biocarbon catalysts produced were characterized in terms of elemental composition before and after deNO$_x$ experiments at 500 °C (Table 1). The results showed higher C content for willow-based than for fern-based catalysts, which was coherent with their biomass type (woody vs. herbaceous) [47,55]. Impregnation of both Ni and Fe resulted in a decrease in the organic composition of biocarbon, of at most 20 wt.% C when heavily impregnated. A slight increase of C content was generally observed after deNO$_x$ experiments due to thermal decomposition, the total observed mass loss being around 5 to 10%.

Table 1
CHNS elemental composition of biocarbon catalysts characterized before and after 500 °C deNO$_x$ experiments.

Sample	Biomass	Metal	deNO$_x$	C	H	N	S
				(wt.%, dry basis/db)			
RF	Fern	None	Fresh	72.78	0.93	1.47	< 0.01
			Spent	70.92	1.00	1.52	< 0.01
FNi	Fern	Ni	Fresh	71.23	0.73	1.86	< 0.01
			Spent	72.78	0.83	1.57	< 0.01
FNi*	Fern	Ni	Fresh	54.68	0.86	1.28	< 0.01
			Spent	57.66	0.52	1.22	< 0.01
FFe	Fern	Fe	Fresh	71.01	0.49	1.07	< 0.01
			Spent	72.05	0.51	0.94	< 0.01
FFe*	Fern	Fe	Fresh	52.43	0.47	0.74	< 0.01
			Spent	53.36	0.38	0.71	< 0.01
FNiFe	Fern	Ni,Fe	Fresh	66.99	0.84	1.15	< 0.01
			Spent	72.28	0.52	1.16	< 0.01
RW	Willow	None	Fresh	80.07	1.32	0.81	< 0.01
			Spent	83.22	1.24	0.89	< 0.01
WNi	Willow	Ni	Fresh	80.34	0.73	0.71	< 0.01
			Spent	87.14	0.51	0.85	< 0.01
WFe	Willow	Fe	Fresh	82.55	0.74	0.62	< 0.01
			Spent	86.12	0.69	0.67	< 0.01

The inorganic composition of biocarbon catalysts were based on ICP-AES analysis (Table 2). Raw biocarbon (RF and RW) had negligible content of Fe and Ni, while the impregnation brought the value above the thresholds of hyperaccumulation (> 0.3 wt.% biocarbon) [45,56]. Both RF and RW biocarbon had high alkaline and alkali-earth (AAEM) content: RF was especially rich in K and had high content of Na, Mg and Ca; while RW was especially rich in Ca and had high content of K. Impregnation with Ni and Fe salts resulted in the leaching of inherent AAEM, which may impact catalytic performance. AAEM ions have been proved to be effective in promoting the deNO$_x$ activity for many simple metal oxides [2]. They play multiple roles including increasing the surface area, creating basic sites to promote NO adsorption, facilitating the desorption of O_2 and forming active sites, leading to enhanced activity [2]. Therefore, AAEM can be seen as inherent metals that may

Table 2
Inorganic composition of biocarbon catalysts before $deNO_x$ experiments.

Sample	Fe	Ni	K	Na	Mg	Ca	Si	Ash content (wt.%, db)
	(wt.% in biocarbon)							
RF	< 0.1	< 0.1	1,9	0,4	0.3	0.9	1.7	14.4
FNi	< 0.1	8,6	< 0.1	< 0.1	< 0.1	0,4	2.3	20.4
FNi*	< 0.1	38.0	1,2	0.2	0.2	0.8	2.2	46.6[1]
FFe	13,2	< 0.1	0,4	0.1	< 0.1	0.3	4.4	28.1
FFe*	64,2	< 0.1	0,9	0.2	0.2	0.8	3.6	76.2[1]
FNiFe	10,3	8,1	0,4	< 0.1	0,1	0.5	4.6	26.2[1]
RW	< 0.1	< 0.1	0,7	< 0.1	0.2	2.3	0.1	6.7
WNi	< 0.1	2,4	0,2	< 0.1	< 0.1	0.7	< 0.1	10.1
WFe	4,6	< 0.1	0,1	< 0.1	< 0.1	0.1	< 0.1	16.7

1. Estimated ash content based on sum of inorganic composition (average moisture content: 8.5 wt.%).

present a catalytic activity for $deNO_x$. Si content is very high in fern biocarbon, compared to the relatively small content in willow biocarbon, which is caused by the nature of biomass. SiO_2 is an inhibitor for $deNO_x$. It can deactivate the inherent K by forming K-silicate in pores and encapsulates active sites, which reduces the accessibility to active sites, thus reducing catalytic activity [57]. Additionally, the increase in Ni and Fe content helps catalyze pyrolysis and dilutes the organic content by increasing inorganic mass [58]. Both could explain the decrease in organic content (Table 1) and the decrease seems more important as inorganic content is high (FFe* and FNi* compared to RF).

3.1.2. *Surface characterization*

The biocarbon catalysts were characterized in terms of specific surface area and porosity type through BET analysis under N_2. Furthermore, the surface chemical groups were analyzed through temperature programmed desorption (TPD, NH_3), oxidation (TPO, CO_2) and reduction (TPR, H_2) (Table 3, spectra in Supporting Information, **Figs. A.1–3**).

The quantity of chemical surface groups and specific surface area are lower for RF biocarbon than for RW biocarbon. Lower specific surface of RF biocarbon (8.8 m^2/g) could be due to lower volatile matter content in reported herbaceous type biomass resulting in less porosity generated during pyrolysis and therefore less specific surface area [55,59,60]. Impregnation impacts little the chemical adsorption, as the total adsorption of three gases (NH_3, CO_2 and H_2) are similar as long as the biocarbon composition remains the same. However, biocarbon impregnated with both Ni and Fe showed higher specific surface area (> 150 m^2/g) than raw biocarbon (< 50 m^2/g), which was also observed in previous studies [61]. This increase could be attributed to the intensifying volatile release during pyrolysis, resulting in the formation of internal porous structure, while the presence of Ni and Fe (Table 2) catalyzes this process [62,63]. Introduction of metals onto the biocarbon could lead to a blocking of pores that reduces access to surface area and adsorption sites for gas (Table 3, FFe*) [64]. Indeed, a loss of pores induces a decrease in surface area. If increased, then porosity is developed and can reflect better access to adsorption sites and could result in higher adsorbed gases. This increase due to impregnation is however not as noticeable compared to the difference in adsorption between fern and willow biocarbon. This means that the surface groups that the biocarbon develops during pyrolysis could have a higher impact on the adsorption of gases than the presence of metals. Therefore, the combination of highly dispersed active sites that perform $deNO_x$ and the omnipresence of NO adsorption sites provided by the surrounding biocarbon could possibly result in high performance. Additionally, metal impregnation (FNi*) could also promote the aromatization of the biocarbon which when coupled with the formation of reduced metallic Ni, agglomerated or nanoparticle, during biomass pyrolysis results in less O-containing sites and may explain a reduction in H_2 adsorption (Table 3) [65–67].

Imagery of the catalysts was also performed through SEM (Fig. 3). Dispersion of metals was observable for willow biocarbon but not for fern biocarbon due to the higher metal content and their lack of discernible feature (dots of Ni). This lack of distinctive structure could be indicative of agglomerated metals and could explain lesser activity and gas adsorption capabilities on behalf of the fern biocarbon (Table 3). However, fern biocarbon possesses higher inorganic content (Table 2) which could be beneficial to $deNO_x$. It was also possible to see some exposed inherent metals from the structure of willow and is associated with wood bark [61,68]. It was also noted that some metals may be covered by a sheet of carbon that could result in loss of active sites (Fig. 4). This sheet could have been formed during pyrolysis and deposited on the reactive metals, and could induce loss in reactive sites and gas adsorption capabilities without losing specific surface area [69]. This could also be a possible source of C for selective reduction of NO or a reduction source for oxidized metals (**Eq.**13) [70].

3.2. *$deNO_x$ experiments*

3.2.1. *$deNO_x$ performance: NO analysis*

The concentration of NO and NO_2 was analyzed on-line every minute (in ppm). No significant production of NO_2 was observed (**Fig. A.4**, Supporting Information) during the experiments conducted and it may be due to its formation mechanism being hindered by NO saturation of the catalyst active sites [71]. Therefore, only X_{NO} was calculated and averaged in 15 min (Fig. 5), which indicated the overall $deNO_x$ performance of different biocarbon catalysts. For all the samples, X_{NO} did not significantly change after 50 min and became almost stable after 75 min. Therefore, the averaging X_{NO} from 75 to 90 min was defined as the steady state X_{NO} (indicated at the curves ends in the corresponding figures).

The values obtained for X_{NO} reaching at most 30.6% (500 °C, gas hourly space velocity of 8235 h^{-1}, direct NO decomposition) could seem insignificant. However, literature on biocarbon for NO_x reduction is

Table 3
Surface chemical groups and specific surface area of biocarbon catalysts before $deNO_x$.

Sample	TPD-NH_3		TPD-CO_2		TPD-H_2		Specific surface area (m^2/g)
	Total adsorption (mmol/g)	T_{max} (°C)	Total adsorption (mmol/g)	T_{max} (°C)	Total adsorption (mmol/g)	T_{max} (°C)	
RF	0.779	913	12.003	915	2.545	993	8.8
FNi	1.480	912	16.207	920	2.921	986	151.6
FNi*	0.645	939	8.975	934	1.684	999	187.5
FFe	0.553	951	8.258	905	0.158	981	309.6
FFe*	0.485	956	6.360	940	1.657	990	259.4
FNiFe	1.088	923	15.980	924	0.994	1000	367.9
RW	1.460	889	23.288	907	1.501	999	42.4
WNi	1.968	949	25.458	914	0.282	988	419.1
WFe	1.249	960	27.773	935	2.108	985	384.2

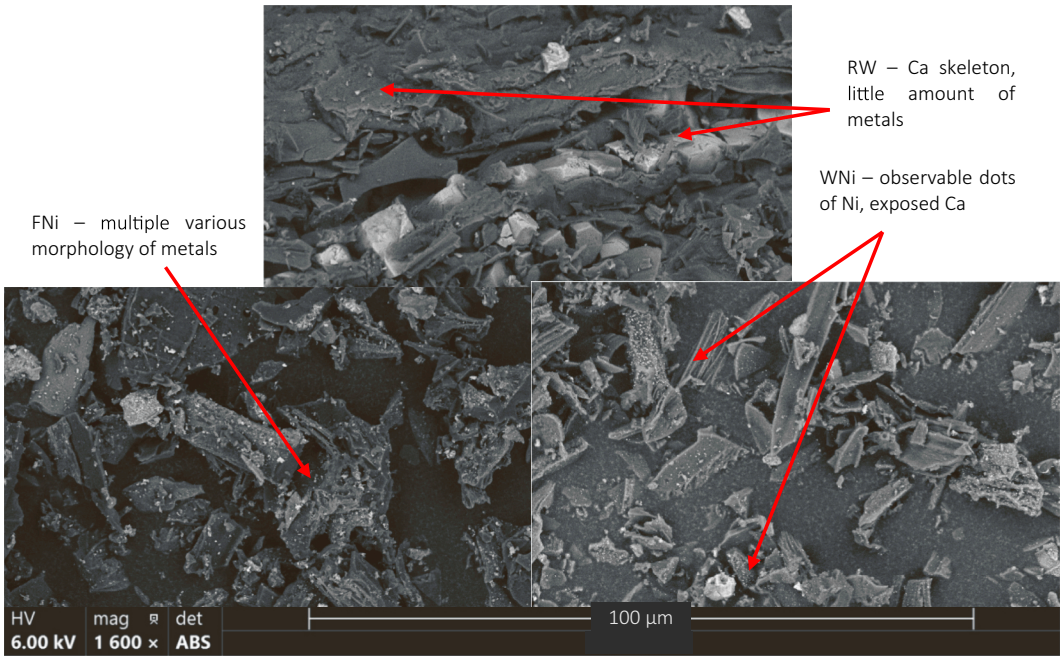

Fig. 3. SEM imagery of different biocarbon catalysts (RW, FNi and WNi biocarbon).

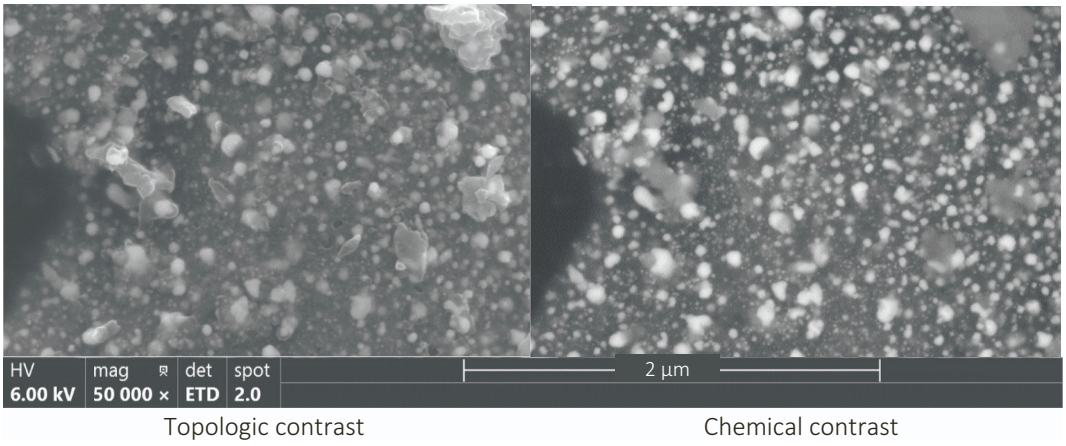

Fig. 4. SEM imagery of FNi biocarbon showing encapsulation of metals.

recent [8,72–74]. Also, most studies concern selective reduction using NH_3, H_2 or CO as a reductant (coupled with O_2) [11,13,22,52]. Indeed, in optimized conditions (200 °C, 16000 h^{-1}, same concentration NO/NH_3 with 5% O_2), NH_3 can improve NO_x reduction capabilities from nearly 0% (no NH_3) to 40% (with NH_3) with biocarbon alone or 90% with N-activated biocarbon-supported perovskite oxide [13]. NH_3 was not used here as it is a health and environmental hazard [75,76].

3.2.1.1. Effects of temperature. Higher temperature has shown promoting effects on the deNO_x performance for all the samples (Fig. 5). The raw biocarbon (RF and RW, Fig. 5a and d) were not fully activated at 200 and 350 °C and had very limited deNO_x effects. Rising temperature to 500 °C significantly enhanced their catalytic activity, as the activation energy needed for the inherent metals was achieved. However, impregnated biocarbon presented a higher X_{NO} with increasing temperature, which should be related to the presence of Fe and Ni (Table 2). This was also shown for WNi (Fig. 5e), except that its performance at 500 °C was the highest (X_{NO} = 30.6%). For FNi (**Fig.** 5b), the performance was close between 350 and 500 °C, both significantly higher than that at 200 °C. This indicated a lower activation temperature for this catalyst for a similar efficiency. This could be related to the high CO_2 adsorption capabilities of willow biocarbon (Table 3) that are related to the capacity to adsorb NO. This adsorption by the surface of the biocarbon means more NO is in contact of active sites and this higher quantity should result in more frequent reaction with NO and therefore higher X_{NO}. For WFe (Fig. 5f), X_{NO} was already high at 200 °C and steadily increased, almost linearly, with temperature, which indicated a wider range of temperature for the use of this catalyst. For FFe (Fig. 5c), similar X_{NO} was achieved at both 200 and 350 °C, both remarkably lower than that at 500 °C. This indicated a higher activation temperature for FFe. Therefore, the high presence of other metals such as AAEM in fern biocarbon did not contribute to diminishing energy barriers and could even be inhibiting at higher temperatures. Then, the gas adsorbing capabilities of willow biocarbon could contribute to its higher performance. Nevertheless, the results show that temperature did increase the deNO_x performance of all biocarbon catalysts.

3.2.1.2. Effects of biomass. The nature of the biomass was an important factor that could influence the effectiveness of the biocarbon catalyst. Indeed, the composition of the initial biomass determined the

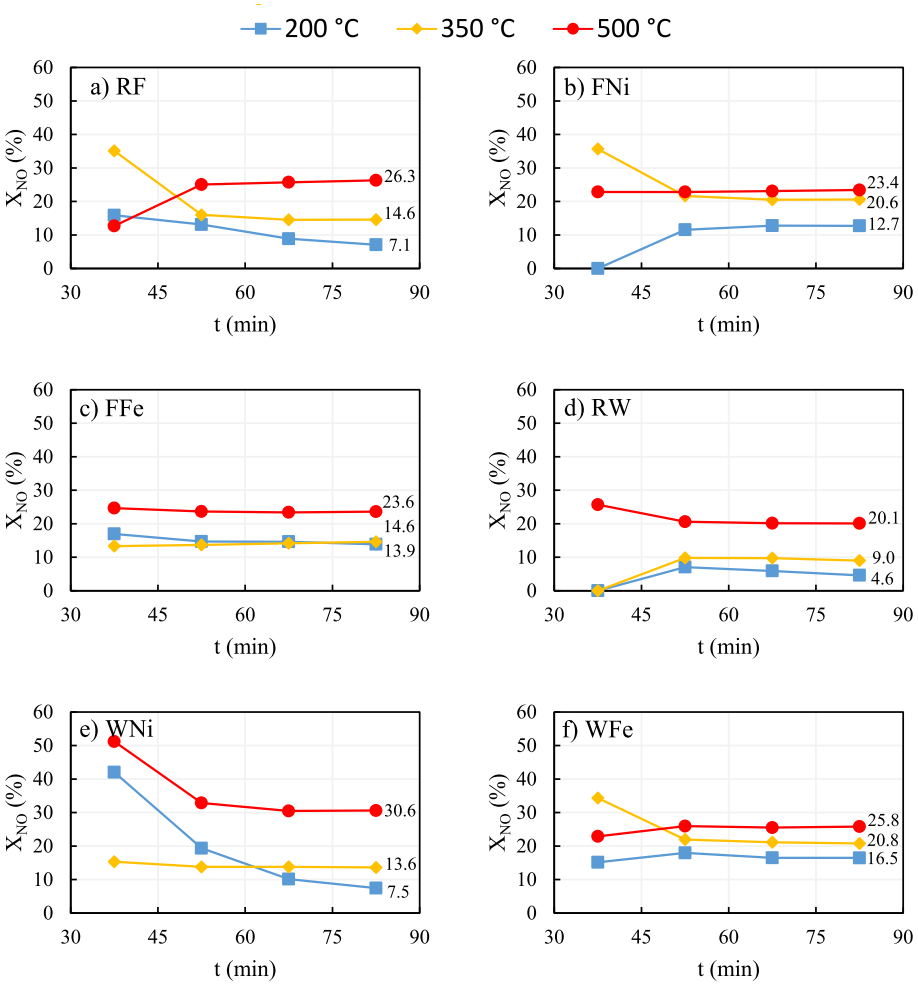

Fig. 5. NO removal ratio X_{NO} of different biocarbon catalysts (RF, FNi, FFe, RW, WNi, WFe) under 1021 ppm NO/Ar.

composition and structure of the biocarbon formed, favorable or not to the NO adsorption and $deNO_x$. In addition, the effectiveness of impregnation may also depend on biomass characteristics. At both 200 and 350 °C, fern biocarbon achieved obviously higher $deNO_x$ performance than their respective willow biocarbon (the only exception is FFe vs. WFe). This was directly relevant to the difference in the inherent metal content of fern and willow, especially K, Na and Mg (Table 2). RF, for example, was significantly better than RW from 200 to 500 °C, which best reflected the influence of biomass and its inherent metals as there was no interference from the impregnated metals. Furthermore, the higher presence of carbon from willow biocarbon (Table 1) could interfere with the small amount of potential active sites (Fig. 4). When impregnated however, the capacity to adsorb higher quantities of NO by the willow-based biocarbon catalysts (Table 3) is highly beneficial to their $deNO_x$ performance.

3.2.1.3. Effects of impregnated metals. The effects of impregnated metals were also important. First of all, impregnation successfully enhanced the performance of the biocarbon catalysts at least at both 200 and 350 °C, as a result of more catalysts available for the adsorption and decomposition. Remarkable examples were FFe at 200 °C (Fig. 5c), and WFe at 200 and 350 °C (Fig. 5f), which at least doubled X_{NO} compared with respective raw biocarbon. According to literature, the $deNO_x$ efficiency of Ni-impregnated and Fe-impregnated active carbon were similar at 300 °C and both significantly higher than that of raw active carbon [77–79]. This also agrees with the fact that metal-loaded carbons show high activity due to the dissociative NO chemisorption [79,80]. In this study, the performance was not always positively correlated to the metal amount because during pyrolysis the impregnated metals could be coated with carbon or aggregated and were therefore not accessible by NO. For example, FNi and FFe (Fig. 5b and c) were both high in their loaded metal content (Table 2), but their performance at 500 °C was worse than the raw biocarbon (RF, Fig. 5a). This was the result of poor availability of metals after pyrolysis at high temperature. For WNi and WFe (Fig. 5e and f), though the loaded metal content was not so high, their performance was better.

To investigate the synergistic effects of Ni and Fe, a bimetallic impregnation was carried out to produce a fern-based biocarbon catalyst containing both Ni and Fe (FNiFe). The $deNO_x$ performance of this sample was compared to that of fern biocarbon (FNi and FFe, Fig. 5b and c). None of the samples achieved better performance than raw biocarbon (RF) at 500 °C. FNi and FFe were close in steady stage X_{NO} (23.4% vs. 23.6%), which were both better than the bimetallic sample, FNiFe (Supporting information, **Fig. A.5**). Therefore, a synergistic effect of Ni and Fe was not found.

3.2.1.4. Effects of metal content. It was revealed above that not only the kind of impregnated metals but also the loaded metals content on biocarbon has significant influence on the $deNO_x$ performance of biocarbon catalysts. Therefore, the behavior of fern-based catalysts with different Ni and Fe content were tested in $deNO_x$ experiments at 200 °C (FFe*, Fig. 6, left) and 500 °C (FNi* and FFe*, Fig. 6).

For FFe, the effects of additional metal content were different at 200 and 500 °C (Fig. 6, left). At 200 °C, FFe* (with 64.17 wt.% Fe) performed

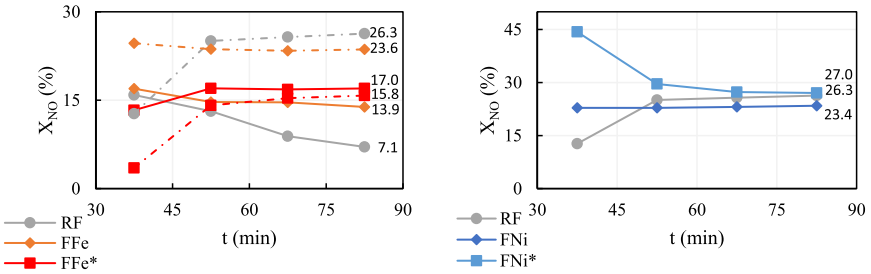

Fig. 6. X_{NO} of fern-based biocarbon catalyst impregnated with higher Fe content and used in $deNO_x$ at 200 (left, full) and 500 °C (left, dotted), and impregnated with higher Ni content and used in $deNO_x$ at 500 °C (right).

slightly better (17.0% > 13.9%) than FFe (with 13.17 wt.% Fe), both significantly better than RF (7.1%). Therefore, higher Fe content (≤ 64 wt.%) could result in better $deNO_x$ performance at 200 °C. At 500 °C, however, highest values of metal content drastically reduced the performance of biocarbon. This indicated the metal blocking of biocarbon pores (Table 3) happened mainly at higher temperature. Therefore, the consideration of optimal metal content to improve $deNO_x$ capabilities might be different depending on the temperature of the emission sources.

In the case of Ni-based catalysts, the steady state X_{NO} of FNi was enhanced from 23.4% to 27.0% at 500 °C when the Ni content was increased from 8.62 wt.% (FNi) to 37.96 wt.% (FNi*, Fig. 6, right). This made its performance slightly better than that of RF. In an industrial application, it needs to be evaluated if the improvement achieved justifies the higher metal cost.

3.2.1.5. Catalyst deactivation. Extended $deNO_x$ experiments (4 h versus 1 h) were conducted to evaluate the catalyst deactivation (Fig. 7), as well as their thermal stability (Table 4).

Within the experimental conditions considered, no significant deactivation of catalysts was observed even in extended $deNO_x$ experiments (Fig. 7), as the NO concentration remained stable after initial transitional stage (30 min), indicating constant $deNO_x$. Therefore, stability could be expected for the biocarbon catalysts in the conditions of the experiment. In terms of thermal stability (Table 4), the impregnated biocarbon seemed to lose <5 wt.% after 1 h $deNO_x$ experiments. The raw biocarbon, however, had a mass loss of 5 to 10 wt.%. This mass loss could be due to reaction with NO, and result in biocarbon surface functional group loss. It could also be linked to CO and CO_2 release during the heating stage [57,81–84]. This could be possibly related to catalyzed pyrolysis that, in addition to reducing organic content (more O and H, Table 1), could stabilize the carbon matrix [85].

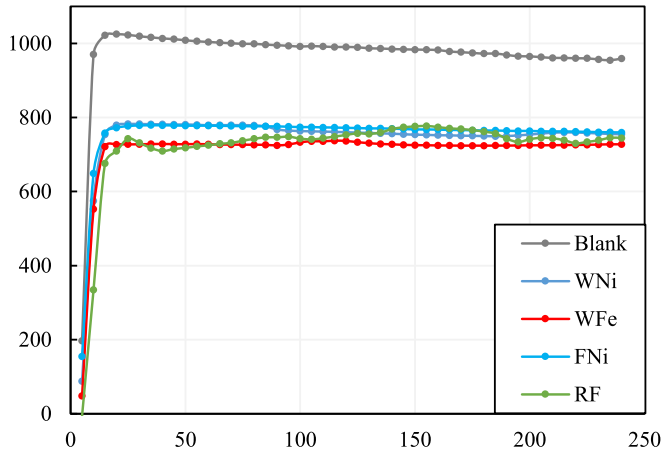

Fig. 7. NO concentration curves of selected biocarbon catalysts (WNi, WFe, FNi, RF and blank test) during 500 °C $deNO_x$ experiments for extended time (4 h), under 1021 ppm NO/Ar.

Table 4
Mass loss of biocarbon catalysts after standard $deNO_x$ experiments (1 h).

T (°C)	RF	FNi	FFe	RW	WNi	WFe
	Mass loss (wt.%, dry basis)					
200	8.6	3.6	3.2	5.9	5.0	3.4
350	6.3	2.8	3.4	7.7	7.6	4.7
500	9.9	4.6	2.1	7.2	4.8	7.2

3.2.2. $deNO_x$ performance through N_2, CO, CO_2 and H_2 fate analysis

3.2.2.1. N_2 fate analysis. Due to the input and replacement of reactor containing biocarbon catalysts at the beginning of each $deNO_x$ experiment, air background is inevitable throughout the experiment. The time needed for gas replacement from gas bottles to μGC analyzer was estimated as 15 min considering the total volume of gas channel. Therefore, the background N_2 concentration ($C_{N_2,BG}$) was calculated by averaging the measured N_2 concentration from t = 30 to 45 min (before the inlet NO gas completely replaced Ar). Then the N_2 concentrations (C_{N_2}) were normalized ($C_{N_2,nor}$) according to this standard to represent the N_2 produced during the test (**Eq**.15).

$$C_{N_2,nor} = C_{N_2} - C_{N_2,BG} \quad \textbf{(15)}$$

The normalized N_2 concentration $C_{N_2,nor}$ can be seen as the indicator of direct decomposition reaction of NO (Fig. 8). In most cases, $C_{N_2,nor}$ was positive during NO phase. Even for those with initial negative values, the curves started to rise after. These indicated that NO is decomposed into N_2 either through direct decomposition or through catalytic reduction (**Eq**.10–12). For RF, the catalyzing performance was enhanced with the increase of temperature, resulting in its higher X_{NO} at higher temperature (Fig. 5). Also, RF performed better than RW, which was related to their difference in inherent metal contents (Table 2). FNi and FFe achieved highest decomposition performance at 200 °C, in contrary to WNi and FFe. This caused their higher X_{NO}, while the NO removed by WNi and WFe was mostly through adsorption at this temperature. With the increase of temperature, both FNi and FFe showed a trend of catalyst deactivation, which should be due to the inhibiting effects of their higher Si content (Table 2), while these did not happen to the respective willow-based biocarbon catalysts (WNi and WFe).

3.2.2.2. CO and CO_2 fate analysis. Selective reduction with biocarbon will lead to the formation of N_2, CO and CO_2 [35], which was also observed in the experiments. This is a side reaction that can cause the degradation of biocarbon.

From the results, the CO_2 evolution followed similar trends among samples (Fig. 9). CO_2 concentration was very high at the beginning and decreased sharply up to 30 min (under Ar). This may be explained by the oxygen groups on biocarbon surface releasing large amounts of CO_2 (Fig. 3). It is fair to assume that the peak of CO_2 should be during the

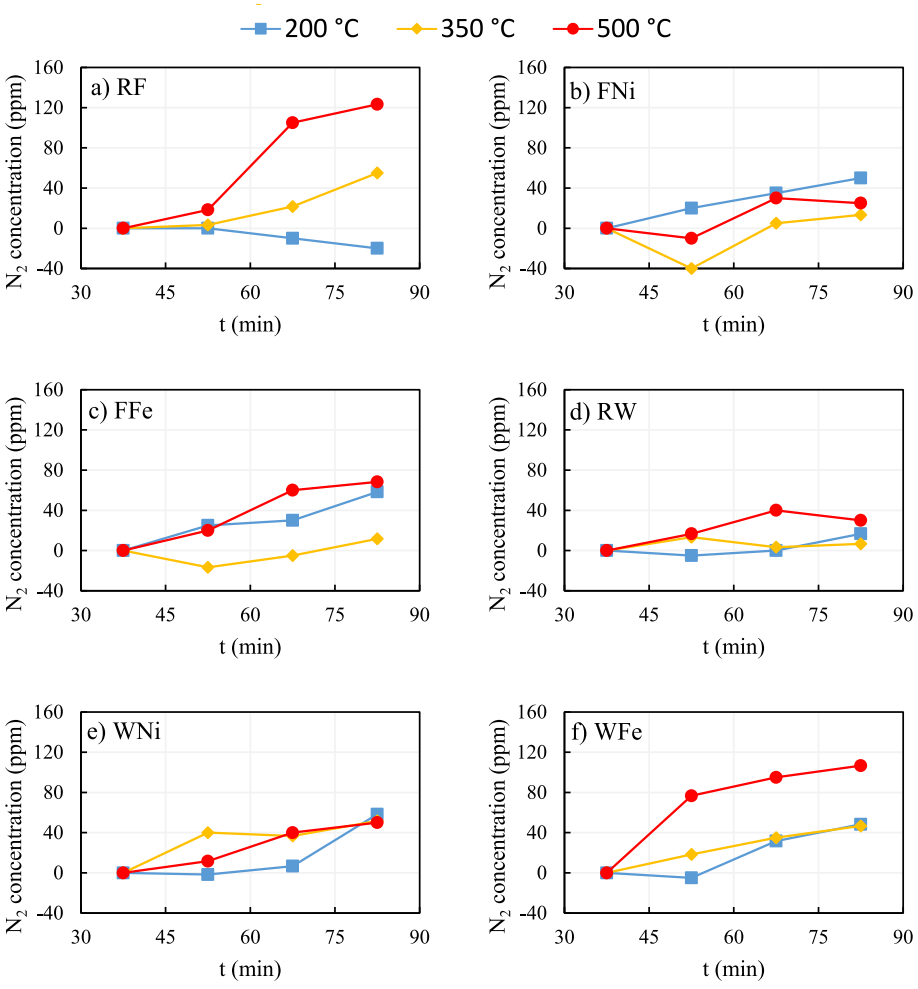

Fig. 8. Normalized N_2 concentration of different biocarbon catalysts (RF, FNi, FFe, RW, WNi, WFe), under 1021 ppm NO/Ar.

temperature rising stage ($t < 0$). In addition, this process was significantly influenced by temperature, as biocarbon released significantly more CO_2 from 350 °C than at 200 °C, which indicated a threshold between 200 and 350 °C. When Ar is switched to NO, CO_2 concentration kept at a low value and steadily decreased. The reasons behind this should be a combination of residue oxygen groups releasing CO_2 and the reduction of NO by biocarbon producing CO_2. This showed that raw biocarbon released more CO_2 than impregnated biocarbon, which corresponded to their higher mass loss (Table 4). This may be an indicator of the supposedly better regenerability of impregnated biocarbon.

Regarding to the CO concentration, there was no CO release at 200 °C and negligible release at 350 °C, therefore only the evolution of CO concentration at 500 °C is presented (Fig. 10). Compared to CO_2, the quantity of CO released was much smaller, indicating CO_2 as the major product of selective reduction reaction. Unlike for CO_2, the impregnated biocarbon released more CO than the raw biocarbon.

3.2.2.3. H_2 fate analysis. H_2 release was not observed at 200 °C, so the evolution of H_2 concentration at 350 and 500 °C was presented (Fig. 11). H_2 release was not so significant at 350 °C and was mostly during the Ar phase. At 500 °C, willow biocarbon released more H_2 than respective fern biocarbon. At both temperatures, almost no H_2 release was found for raw biocarbon.

3.3. Proposed mechanisms

Based on results discussed in this work, a graphical illustration of reported mechanisms for $deNO_x$ was represented (Fig. 12). Additionally, the change in mechanism brought by the presence of metal was also represented. In this work, the metal-based mechanism is likely, with C provided by the biocarbon directly (**Eq.**16–18), but further studies would be needed to confirm this. Other studies mention that, in addition to metallic active sites, O vacancies present on the biocarbon surface or formed during $deNO_x$ through the reduction of O containing functional groups by NO and CO forming NO_2 and CO_2, can serve as adsorption and reaction sites [11,13]. NO_2 can quickly react with CO to form CO_2 and N_2 and may attest to the little production in this study (**Fig. A.1**, Supporting Information) [11]. H_2 may also contribute to NO reduction [22]. Furthermore, only specific functional groups may take part in $deNO_x$ and result in others being spectators or even inhibitors by adsorbing and isolating co-reactants such as CO or NH_3 [11,76]. To increase NO uptake, new research focuses on impregnating biocarbon with metals that present high oxygen storage capacity such as ceria (Ce) or manganese (Mn) [8,72,73].

$deNO_x$ reaction over metal:

$$M + {}^{*} \longrightarrow M^{*} \quad \textbf{(16)}$$

$$2M^{*} + 2NO \longrightarrow 2MO^{*} + N_2 \quad \textbf{(17)}$$

$$xMO^{*} + C \longrightarrow xM^{*} + CO_x \quad \textbf{(18)}$$

4. Conclusions

Lignocellulosic fern and willow impregnated with heavy metals (Ni/

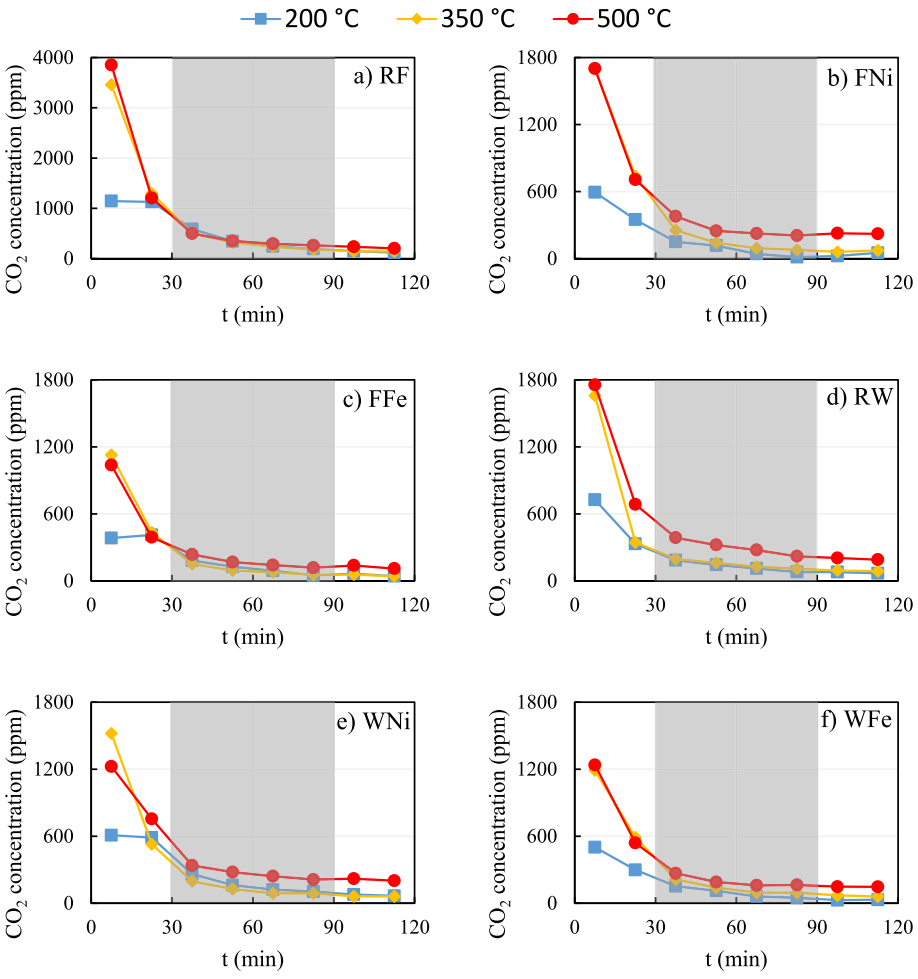

Fig. 9. CO_2 concentration of different biocarbon catalysts (RF, FNi, FFe, RW, WNi, WFe); blank area: Ar, shadow area: 1021 ppm NO/Ar.

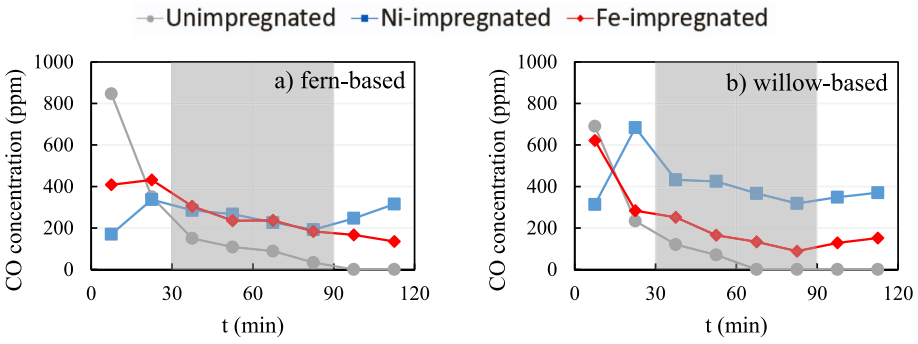

Fig. 10. CO concentration of different biocarbon catalysts during 500 °C $deNO_x$ experiments (a: fern biocarbon; b: willow biocarbon); blank area: Ar, shadow area: 1021 ppm NO/Ar.

Fe) were pyrolyzed (800 °C, N_2) to produce biocarbon catalysts, which showed promising performances in NO decomposition ($deNO_x$) at 200, 350 and 500 °C. Generally, higher temperatures showed better performances but a strict linear correlation was not observed. At 200 and 350 °C, adsorption of NO on biocarbon surface was facilitated by the high specific surface area of impregnated biocarbon (151.6 to 419.1 m^2/g), compared to that of raw biocarbon (< 50 m^2/g). This resulted in a remarkable enhancement of $deNO_x$ performance at this temperature range. At 500 °C, adsorption and decomposition were competing in the $deNO_x$ mechanism, and the inherent metals from raw biocarbon seemed to play an important part. As a result, the effects of impregnated metals were less positive or even negative at this temperature, except for WNi, which achieved a remarkably high $deNO_x$ ratio of 30.6% (10.5% higher than RW). Fern biocarbon achieved higher $deNO_x$ performance than the respective willow biocarbon at both 200 and 350 °C, mostly due to their higher content of inherent metals (K, Na) that could facilitate activity from loaded metals (Ni or Fe). At 500 °C, willow biocarbon could outperform their fern counterparts as the loaded metals could be activated and benefit from the high NO adsorption of the biocarbon. Increasing the metal content generally slightly enhanced their performance in $deNO_x$ at 200 °C, but not significantly at 500 °C, and could justify use of a metal-poor biocarbon. No significant synergistic effects

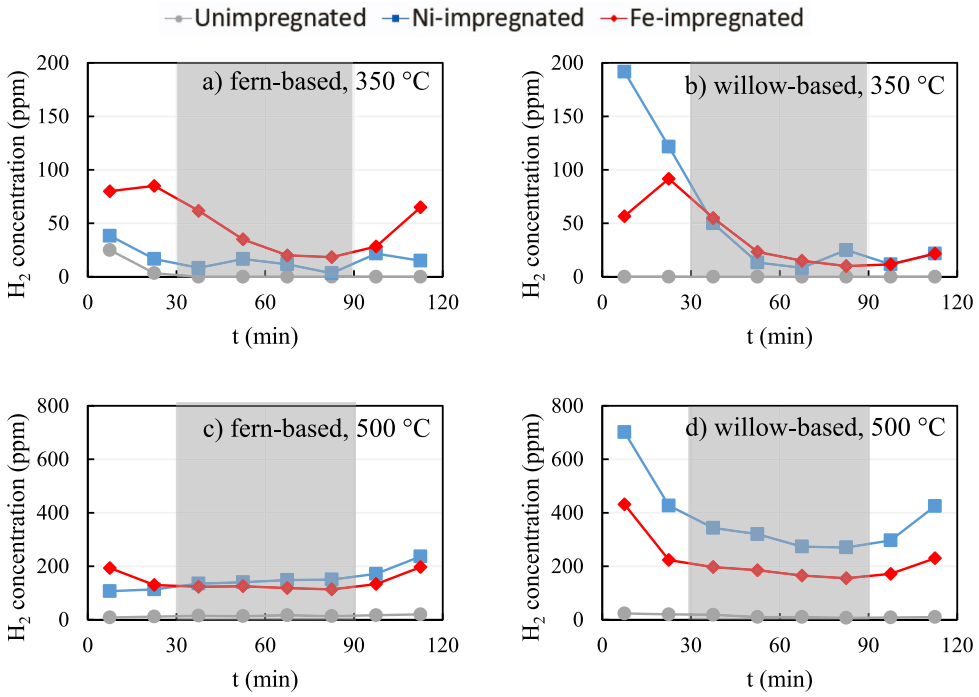

Fig. 11. H_2 concentration of different biocarbon catalysts during 350 (top) and 500 °C (bottom) deNO_x experiments (left: fern biocarbon; right: willow biocarbon); blank area: Ar, shadow area: 1021 ppm NO/Ar.

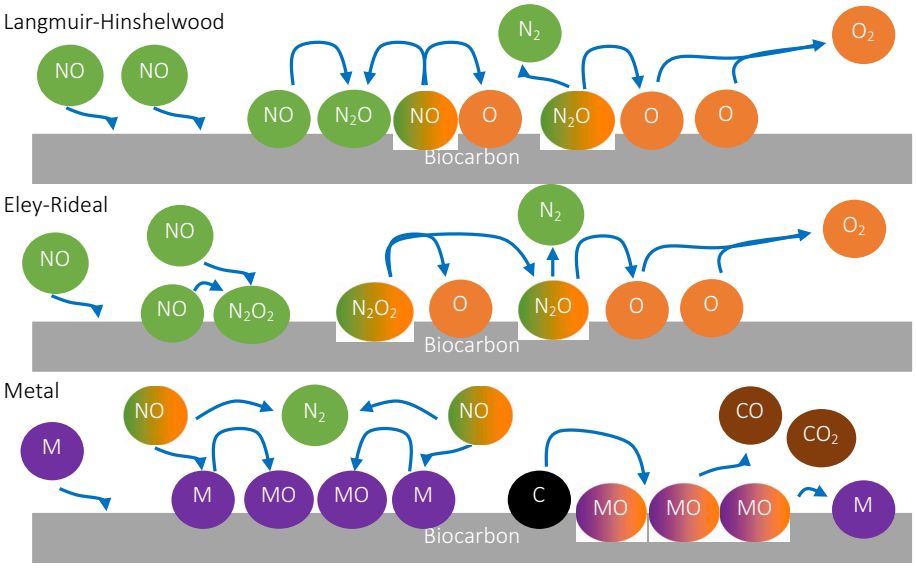

Fig. 12. Graphical representation of deNO_x mechanism reported in literature.

were found with fern biocarbon impregnated with both Ni and Fe.

A production of N_2 was observed during deNO_x experiments under NO flow, suggesting that the direct decomposition of NO was the main reaction, facilitated by higher temperature for most catalysts. The release of CO_2 observed under both Ar and NO flow was mostly from the surface chemical groups on biocarbon surface and peaked at the temperature rising stage (under Ar). The selective reduction of NO with biocarbon also contributed slightly to this release and was a side reaction. CO and H_2 was detected in smaller quantities. The impregnated biocarbon released less gas (CO_2, CO and H_2) than raw biocarbon, resulting in lower mass loss after deNO_x, and suggested better stability and regenerability.

Further work will be carried out to study the influence of activating the biocarbon catalysts and use of a real gaseous effluent containing nitrogen oxides. Furthermore, potential regeneration routes, in addition to longer experimental duration, will be explored to facilitate the upscaling in the use of these biocarbon catalysts as opposed to metal catalysts.

CRediT authorship contribution statement

Théodore Graul: Writing – review & editing, Visualization, Validation, Supervision, Resources, Methodology. **María González Martínez:** Writing – review & editing, Visualization, Validation, Supervision, Resources, Project administration, Funding acquisition. **Yi Qiu:** Writing – original draft, Visualization, Methodology, Investigation, Formal

analysis. **Floriane Fourgeaud:** Writing – review & editing, Visualization, Methodology, Investigation, Formal analysis. **Kuo Zeng:** Writing – review & editing, Validation, Supervision. **Ange Nzihou:** Writing – review & editing, Validation, Supervision, Resources, Project administration, Funding acquisition, Conceptualization.

Declaration of competing interest

The authors declare that they have no known competing financial interests or personal relationships that could have appeared to influence the work reported in this paper.

Data availability

Data will be made available upon reasonable request to the corresponding author.

Acknowledgments

The authors sincerely acknowledge the support provided by Eizhy, which provided shrubland biomass used in this study, as well as the European Union's Horizon 2020 research and innovation program under grant agreement No 637020—MOBILE FLIP for the willow biomass used in this study.

Appendix A. Supplementary data

Supplementary data to this article can be found online at https://doi.org/10.1016/j.apcato.2024.206982.

References

[1] K. Feng, Y. Hu, T. Cao, Mechanism of fuel gas denitration on the KOH-activated biochar surface, J. Phys. Chem. A 126 (2022) 296–305, https://doi.org/10.1021/acs.jpca.1c09518.
[2] P. Xie, W. Ji, Y. Li, C. Zhang, NO direct decomposition: progress, challenges and opportunities, Catal. Sci. Technol. 11 (2021) 374–391, https://doi.org/10.1039/D0CY02041A.
[3] N. Li, Y. Wang, S. Cui, X. Jin, Experimental and kinetic investigation on NO reduction by rice husk char and catalytically with CO, Appl. Sci. 10 (2020) 6715, https://doi.org/10.3390/app10196715.
[4] L. Chen, L. Liu, Y. Zhao, Y. Zhao, R. Sun, S. Sun, P. Qiu, Char structural evolution characteristics and its correlation with reactivity during the heterogeneous NO reduction in a micro fluidized bed reaction analyzer: the influence of reaction atmosphere, Fuel 303 (2021) 121173, https://doi.org/10.1016/j.fuel.2021.121173.
[5] W. Deng, C. Tao, K. Cobb, H. Zhou, Y. Su, R. Ruan, Catalytic oxidation of NO at ambient temperature over the chars from pyrolysis of sewage sludge, Chemosphere 251 (2020) 126429, https://doi.org/10.1016/j.chemosphere.2020.126429.
[6] S. Roy, M.S. Hegde, G. Madras, Catalysis for NOx abatement, Appl. Energy 86 (2009) 2283–2297, https://doi.org/10.1016/j.apenergy.2009.03.022.
[7] L. He, G. Li, X. Wu, S. Zhang, M. Tian, Z. Li, C. Huang, Q. Hu, Y. Wu, J. Hao, Characteristics of NOX and NH3 emissions from in-use heavy-duty diesel vehicles with various aftertreatment technologies in China, J. Hazard. Mater. 465 (2024) 133073, https://doi.org/10.1016/j.jhazmat.2023.133073.
[8] Y. Shi, T. Zhao, J. Du, B. Feng, Q. Tang, S. Shan, M. Zhang, Q. Wang, J. Zhao, Low temperature NH3 selective catalytic reduction of NOx over CeOx-biochar catalyst prepared by air oxidation, J. Energy Inst. 112 (2024) 101484, https://doi.org/10.1016/j.joei.2023.101484.
[9] Q. Sun, Z. Wang, D. Wang, Z. Hong, M. Zhou, X. Li, A review on the catalytic decomposition of NO to N2 and O2: catalysts and processes, Catal. Sci. Technol. 8 (2018) 4563–4575, https://doi.org/10.1039/C8CY01114A.
[10] F. Garin, Mechanism of NOx decomposition, Appl. Catal. A Gen. 222 (2001) 183–219, https://doi.org/10.1016/S0926-860X(01)00827-4.
[11] Z. Gholami, G. Luo, F. Gholami, The influence of support composition on the activity of Cu:Ce catalysts for selective catalytic reduction of NO by CO in the presence of excess oxygen, New J. Chem. 44 (2020) 709–718, https://doi.org/10.1039/C9NJ04335G.
[12] M.A. Vannice, A.B. Walters, X. Zhang, The kinetics of NOxDecomposition and NO reduction by CH4overLa2O3and Sr/La2O3, J. Catal. 159 (1996) 119–126, https://doi.org/10.1006/jcat.1996.0071.
[13] X. Fan, L. Hao, X. Gu, S. Li, Low-temperature selective catalytic reduction of NO with NH3 over a biochar-supported perovskite oxide catalyst, Energy Fuel 37 (2023) 7339–7352, https://doi.org/10.1021/acs.energyfuels.2c04291.
[14] S. Pancharatnam, K.J. Lim, D.M. Mason, The decomposition of nitric oxide on a heated platinum wire, Chem. Eng. Sci. 30 (1975) 781–787, https://doi.org/10.1016/0009-2509(75)80042-X.
[15] A. Ogata, A. Obuchi, K. Mizuno, A. Ohi, H. Aoyama, H. Ohuchi, Enhancement effect of Mg2+ ion on direct nitric oxide decomposition over supported palladium catalysts, Appl. Catal. 65 (1990) L11–L15, https://doi.org/10.1016/S0166-9834(00)81582-1.
[16] T.E. Green, C.N. Hinshelwood, CCXXIV.—the catalytic decomposition of nitric oxide at the surface of platinum, J. Chem. Soc. 129 (1926) 1709–1713, https://doi.org/10.1039/JR9262901709.
[17] A. Gervasini, P. Carniti, V. Ragaini, Studies of direct decomposition and reduction of nitrogen oxide with ethylene by supported noble metal catalysts, Appl. Catal. B Environ. 22 (1999) 201–213, https://doi.org/10.1016/S0926-3373(99)00053-3.
[18] R. Li, Y. Li, Z. Liu, Recent advances in the catalytic removal of NOx and N2O over spinel oxide-based catalyst, Fuel 355 (2024) 129405, https://doi.org/10.1016/j.fuel.2023.129405.
[19] J.M. Fraser, F. Daniels, The heterogeneous decomposition of nitric oxide with oxide catalysts, J. Phys. Chem. 62 (1958) 215–219, https://doi.org/10.1021/j150560a017.
[20] M. Shelef, K. Otto, H. Gandhi, The heterogeneous decomposition of nitric oxide on supported catalysts, Atmos. Environ. 3 (1969) (1967) 107–122, https://doi.org/10.1016/0004-6981(69)90002-X.
[21] S. Xie, G. Mestl, M.P. Rosynek, J.H. Lunsford, Decomposition of nitric oxide over barium oxide supported on magnesium oxide. 1. Catalytic results and in situ Raman spectroscopic evidence for a barium—nitro intermediate, J. Am. Chem. Soc. 119 (1997) 10186–10191, https://doi.org/10.1021/ja970809k.
[22] I. Yakub, K.A. Mohamad Said, R. Baini, M.A. Mohamed Amin, Enhancing the catalytic properties of a biochar-supported copper oxide in nitric oxide selective reduction with hydrogen, Braz. J. Chem. Eng. (2024), https://doi.org/10.1007/s43153-024-00453-z.
[23] N. Imanaka, T. Masui, H. Masaki, Direct decomposition of nitric oxide over C-type cubic (Gd1–x–yYxBay)2O3–y solid solutions, Adv. Mater. 19 (2007) 3660–3663, https://doi.org/10.1002/adma.200602323.
[24] S. Tsujimoto, K. Yasuda, T. Masui, N. Imanaka, Effects of Tb and Ba introduction on the reaction mechanism of direct NO decomposition over C-type cubic rare earth oxides based on Y2O3, Catal. Sci. Technol. 3 (2013) 1928–1936, https://doi.org/10.1039/C3CY20746C.
[25] Y. Teraoka, H. Fukuda, S. Kagawa, Catalytic activity of perovskite-type oxides for the direct decomposition of nitrogen monoxide, Chem. Lett. 19 (1990) 1–4, https://doi.org/10.1246/cl.1990.1.
[26] S. Fang, A. Takagaki, M. Watanabe, T. Ishihara, The direct decomposition of NO into N2 and O2 over copper doped Ba3Y4O9, Catal, Sci. Technol. 10 (2020) 2513–2522, https://doi.org/10.1039/D0CY00194E.
[27] P. Xie, X. Yong, M. Wei, Y. Li, C. Zhang, High performance catalysts BaCoO3—CeO2 prepared by the one-pot method for NO direct decomposition, ChemCatChem 12 (2020) 4297–4303, https://doi.org/10.1002/cctc.202000701.
[28] S. Kagawa, S. Yoko-o, M. Iwamoto, Activity of copper (II)-exchanged Y-type zeolites in the catalytic decomposition of nitrogen monoxide, J. Chem. Soc. Chem. Commun. 0 (1978) 1058–1059, https://doi.org/10.1039/C39780001058.
[29] M. Iwamoto, H. Furukawa, Y. Mine, F. Uemura, S. Mikuriya, S. Kagawa, Copper(II) ion-exchanged ZSM-5 zeolites as highly active catalysts for direct and continuous decomposition of nitrogen monoxide, J. Chem. Soc. Chem. Commun. (1986) 1272–1273, https://doi.org/10.1039/C39860001272.
[30] L. Chen, S. Ren, Y. Jiang, L. Liu, M. Wang, J. Yang, Z. Chen, W. Liu, Q. Liu, Effect of Mn and Ce oxides on low-temperature NH3-SCR performance over blast furnace slag-derived zeolite X supported catalysts, Fuel 320 (2022) 123969, https://doi.org/10.1016/j.fuel.2022.123969.
[31] Y. Wang, Y. Shen, Y. Zhou, Z. Xue, Z. Xi, S. Zhu, Heteroatom-doped graphene for efficient NO decomposition by metal-free catalysis, ACS Appl. Mater. Interfaces 10 (2018) 36202–36210, https://doi.org/10.1021/acsami.8b09503.
[32] N. Imanaka, T. Masui, Advances in direct NOx decomposition catalysts, Appl. Catal. A Gen. 431–432 (2012) 1–8, https://doi.org/10.1016/j.apcata.2012.02.047.
[33] X. Li, H. Wang, G. Shao, G. Wang, L. Lu, Low temperature reduction of NO by activated carbons impregnated with Fe based catalysts, Int. J. Hydrog. Energy 44 (2019) 25265–25275, https://doi.org/10.1016/j.ijhydene.2019.04.008.
[34] X. Cheng, X. Zhang, M. Zhang, P. Sun, Z. Wang, C. Ma, A simulated rotary reactor for NOx reduction by carbon monoxide over Fe/ZSM-5 catalysts, Chem. Eng. J. 307 (2017) 24–40, https://doi.org/10.1016/j.cej.2016.08.076.
[35] Y. Shu, F. Zhang, F. Wang, H. Wang, Catalytic reduction of NOx by biomass-derived activated carbon supported metals, Chin. J. Chem. Eng. 26 (2018) 2077–2083, https://doi.org/10.1016/j.cjche.2018.04.019.
[36] S. Ning, Y. Su, W. Deng, B. Zhao, Fe-Ni bimetallic atomic catalysts supported on ZIF-8 derived carbon for C3H6-SCR of NO: catalytic performance and reaction mechanism, Sep. Purif. Technol. 335 (2024) 126207, https://doi.org/10.1016/j.seppur.2023.126207.
[37] J. Lee, K.-H. Kim, E.E. Kwon, Biochar as a catalyst, Renew. Sust. Energ. Rev. 77 (2017) 70–79, https://doi.org/10.1016/j.rser.2017.04.002.
[38] S. Younis, K.-H. Kim, Recent advances in biochar-based catalysts: air purification and opportunities for industrial upscaling, Asian J. Atmos. Environ. 16 (2022) 104–120, https://doi.org/10.5572/ajae.2022.117.
[39] N. Bolan, S.A. Hoang, J. Beiyuan, S. Gupta, D. Hou, A. Karakoti, S. Joseph, S. Jung, K.-H. Kim, M.B. Kirkham, H.W. Kua, M. Kumar, E.E. Kwon, Y.S. Ok, V. Perera, J. Rinklebe, S.M. Shaheen, B. Sarkar, A.K. Sarmah, B.P. Singh, G. Singh, D.C. W. Tsang, K. Vikrant, M. Vithanage, A. Vinu, H. Wang, H. Wijesekara, Y. Yan, S. A. Younis, L. Van Zwieten, Multifunctional applications of biochar beyond carbon

storage, Int. Mater. Rev. 67 (2022) 150–200, https://doi.org/10.1080/09506608.2021.1922047.
[40] T. Graul, M. Gonzalez Martinez, A. Nzihou, Nickel and iron-doped biocarbon catalysts for reverse water-gas shift reaction, ChemCatChem (2024), https://doi.org/10.1002/cctc.202301398 e202301398.
[41] X.Y. Wu, Q. Song, H.B. Zhao, Z.H. Zhang, Q. Yao, Kinetic modeling of inherent mineral catalyzed NO reduction by biomass char, Environ. Sci. Technol. 48 (2014) 4184–4190, https://doi.org/10.1021/es405521k.
[42] K. Zhao, X. Sun, C. Wang, X. Song, F. Wang, K. Li, P. Ning, Supported catalysts for simultaneous removal of SO2, NOx, and Hg0 from industrial exhaust gases: a review, Chin. Chem. Lett. 32 (2021) 2963–2974, https://doi.org/10.1016/j.cclet.2021.03.023.
[43] P.Y.R. Suzaki, M.T. Munaro, C.C. Triques, S.J. Kleinübing, M.R.F. Klen, L.M. de Matos Jorge, R. Bergamasco, Biosorption of binary heavy metal systems: phenomenological mathematical modeling, Chem. Eng. J. 313 (2017) 364–373, https://doi.org/10.1016/j.cej.2016.12.082.
[44] W.-J. Liu, W.-W. Li, H. Jiang, H.-Q. Yu, Fates of chemical elements in biomass during its pyrolysis, Chem. Rev. 117 (2017) 6367–6398, https://doi.org/10.1021/acs.chemrev.6b00647.
[45] W. Su, X. Li, H. Zhang, Y. Xing, P. Liu, C. Cai, Migration and transformation of heavy metals in hyperaccumulators during the thermal treatment: a review, Environ. Sci. Pollut. Res. 28 (2021) 47838–47855, https://doi.org/10.1007/s11356-021-15346-8.
[46] T. Do Minh, J. Song, A. Deb, L. Cha, V. Srivastava, M. Sillanpää, Biochar based catalysts for the abatement of emerging pollutants: a review, Chem. Eng. J. 394 (2020) 124856, https://doi.org/10.1016/j.cej.2020.124856.
[47] M. González Martínez, C. Dupont, D. da Silva Perez, L. Míguez-Rodríguez, M. Grateau, S. Thiéry, T. Tamminen, X.-M. Meyer, C. Gourdon, Assessing the suitability of recovering shrub biowaste involved in wildland fires in the South of Europe through torrefaction mobile units, J. Environ. Manag. 236 (2019) 551–560, https://doi.org/10.1016/j.jenvman.2019.02.019.
[48] W.-X. Peng, X. Yue, H. Chen, N.L. Ma, Z. Quan, Q. Yu, Z. Wei, R. Guan, S.S. Lam, J. Rinklebe, D. Zhang, B. Zhang, N. Bolan, M.B. Kirkham, C. Sonne, A review of plants formaldehyde metabolism: implications for hazardous emissions and phytoremediation, J. Hazard. Mater. 436 (2022) 129304, https://doi.org/10.1016/j.jhazmat.2022.129304.
[49] M. Lawrinenko, Z. Wang, R. Horton, D. Mendivelso-Perez, E.A. Smith, T. E. Webster, D.A. Laird, J.H. van Leeuwen, Macroporous carbon supported zerovalent iron for remediation of trichloroethylene, ACS Sustain. Chem. Eng. 5 (2017) 1586–1593, https://doi.org/10.1021/acssuschemeng.6b02375.
[50] M. Said, Comportements et rôles des métaux lourds au cours de la pyro-gazéification de la biomasse: Études expérimentales et thermodynamiques, phdthesis, Ecole des Mines d'Albi-Carmaux, 2016, https://tel.archives-ouvertes.fr/tel-01541337 (accessed June 9, 2021).
[51] S.A. Dastgheib, H. Salih, T. Ilangovan, J. Mock, NO oxidation by activated carbon catalysts: impact of carbon characteristics, pressure, and the presence of water, ACS Omega 5 (2020) 21172–21180, https://doi.org/10.1021/acsomega.0c02891.
[52] S.I. Anthonysamy, P. Lahijani, M. Mohammadi, A. Mohamed, Dynamic adsorption of nitric oxide (NO) in a fixed-bed reactor using rubber seed shell-derived biochar, biointerface research in applied, Chemistry 12 (2021) 1638–1650, https://doi.org/10.33263/BRIAC122.16381650.
[53] Z. Zhu, Z. Liu, S. Liu, H. Niu, Adsorption and reduction of NO over activated coke at low temperature, Fuel 79 (2000) 651–658, https://doi.org/10.1016/S0016-2361(99)00192-1.
[54] J. Zawadzki, M. Wiśniewski, Adsorption and decomposition of NO on carbon and carbon-supported catalysts, Carbon 40 (2002) 119–124, https://doi.org/10.1016/S0008-6223(01)00081-1.
[55] S.V. Vassilev, D. Baxter, L.K. Andersen, C.G. Vassileva, An overview of the chemical composition of biomass, Fuel 89 (2010) 913–933, https://doi.org/10.1016/j.fuel.2009.10.022.
[56] R.D. Reeves, A.J.M. Baker, T. Jaffré, P.D. Erskine, G. Echevarria, A. van der Ent, A global database for plants that hyperaccumulate metal and metalloid trace elements, New Phytol. 218 (2018) 407–411.
[57] M. Hervy, Valorisation de chars issus de pyrogazéification de biomasse pour la purification de syngas: Lien entre propriétés physico-chimiques, procédé de fonctionnalisation et efficacité du traitement, These de doctorat, Ecole nationale des Mines d'Albi-Carmaux, 2016, http://www.theses.fr/2016EMAC0013 (accessed June 15, 2021).
[58] E. Leng, Y. Guo, J. Chen, S. Liu, J. E, Y. Xue, A comprehensive review on lignin pyrolysis: mechanism, modeling and the effects of inherent metals in biomass, Fuel 309 (2022) 122102, https://doi.org/10.1016/j.fuel.2021.122102.
[59] M. González Martínez, C. Dupont, A. Anca-Couce, D. da Silva Perez, G. Boissonnet, S. Thiéry, X.M. Meyer, C. Gourdon, Understanding the torrefaction of woody and agricultural biomasses through their extracted macromolecular components. Part 2: Torrefaction model, Energy 210 (118451) (2020) 1–18, https://doi.org/10.1016/j.energy.2020.118451.
[60] A. Mukherjee, A.R. Zimmerman, W. Harris, Surface chemistry variations among a series of laboratory-produced biochars, Geoderma 163 (2011) 247–255, https://doi.org/10.1016/j.geoderma.2011.04.021.
[61] K. Zeng, R. Li, D.P. Minh, E. Weiss-Hortala, A. Nzihou, D. Zhong, G. Flamant, Characterization of char generated from solar pyrolysis of heavy metal contaminated biomass, Energy 206 (2020) 118128, https://doi.org/10.1016/j.energy.2020.118128.
[62] R. Li, H. Huang, J.J. Wang, W. Liang, P. Gao, Z. Zhang, R. Xiao, B. Zhou, X. Zhang, Conversion of Cu(II)-polluted biomass into an environmentally benign Cu nanoparticles-embedded biochar composite and its potential use on cyanobacteria inhibition, J. Clean. Prod. 216 (2019) 25–32, https://doi.org/10.1016/j.jclepro.2019.01.186.
[63] S. Xia, K. Li, H. Xiao, N. Cai, Z. Dong, C. Xu, Y. Chen, H. Yang, X. Tu, H. Chen, Pyrolysis of Chinese chestnut shells: effects of temperature and Fe presence on product composition, Bioresour. Technol. 287 (2019) 121444, https://doi.org/10.1016/j.biortech.2019.121444.
[64] D. Akhil, D. Lakshmi, A. Kartik, D.-V.N. Vo, J. Arun, K.P. Gopinath, Production, characterization, activation and environmental applications of engineered biochar: a review, Environ. Chem. Lett. 19 (2021) 2261–2297, https://doi.org/10.1007/s10311-020-01167-7.
[65] M. Fan, Y. Shao, C. Li, F. Mérimé Bkangmo Kontchouo, W. Ren, S. Zhang, S. Wang, B. Li, X. Hu, Balanced anchoring sites and volatile matter in biochar render Ni/biochar with higher metal dispersion and superior activity in hydrogenation of vanillin, Fuel 357 (2024) 129923, https://doi.org/10.1016/j.fuel.2023.129923.
[66] İ. Demiral, C. Samdan, H. Demiral, Enrichment of the surface functional groups of activated carbon by modification method, Surfaces and Interfaces 22 (2021) 100873, https://doi.org/10.1016/j.surfin.2020.100873.
[67] Z.-Y. Du, Z.-H. Zhang, C. Xu, X.-B. Wang, W.-Y. Li, Low-temperature steam reforming of toluene and biomass tar over biochar-supported Ni nanoparticles, ACS Sustain. Chem. Eng. 7 (2019) 3111–3119, https://doi.org/10.1021/acssuschemeng.8b04872.
[68] B.C. Hanger, The movement of calcium in plants, Commun. Soil Sci. Plant Anal. 10 (1979) 171–193, https://doi.org/10.1080/00103627909366887.
[69] D. Feng, Y. Zhang, Y. Zhao, S. Sun, J. Gao, Improvement and maintenance of biochar catalytic activity for in-situ biomass tar reforming during pyrolysis and H2O/CO2 gasification, Fuel Process. Technol. 172 (2018) 106–114, https://doi.org/10.1016/j.fuproc.2017.12.011.
[70] Z. Gholami, G. Luo, F. Gholami, F. Yang, Recent advances in selective catalytic reduction of NOx by carbon monoxide for flue gas cleaning process: a review, Catal. Rev. 63 (2021) 68–119, https://doi.org/10.1080/01614940.2020.1753972.
[71] Z. Liu, C. Chen, J. Zhao, L. Yang, K. Sun, L. Zeng, Y. Pan, Y. Liu, C. Liu, Study on the NO2 production pathways and the role of NO2 in fast selective catalytic reduction DeNOx at low-temperature over MnOx/TiO2 catalyst, Chem. Eng. J. 379 (2020) 122288, https://doi.org/10.1016/j.cej.2019.122288.
[72] S. Raja, D. Eshwar, S. Natarajan, A. Madraswala, C.M. Bharath Babu, M.S. Alphin, S. Manigandan, Biochar supported manganese based catalyst for low-temperature selective catalytic reduction of nitric oxide, Clean Techn. Environ. Policy 25 (2023) 1109–1118, https://doi.org/10.1007/s10098-022-02274-5.
[73] S.I. Anthonysamy, P. Lahijani, M. Mohammadi, A.R. Mohamed, Low temperature adsorption of nitric oxide on cerium impregnated biomass-derived biochar, Korean J. Chem. Eng. 37 (2020) 130–140, https://doi.org/10.1007/s11814-019-0405-9.
[74] Q.-C. Gong, L.-Q. He, L.-H. Zhang, F. Duan, Comparison of the NO heterogeneous reduction characteristics using biochars derived from three biomass with different lignin types, J. Environ. Chem. Eng. 9 (2021) 105020, https://doi.org/10.1016/j.jece.2020.105020.
[75] B. Gu, L. Zhang, R. Van Dingenen, M. Vieno, H.J. Van Grinsven, X. Zhang, S. Zhang, Y. Chen, S. Wang, C. Ren, S. Rao, M. Holland, W. Winiwarter, D. Chen, J. Xu, M. A. Sutton, Abating ammonia is more cost-effective than nitrogen oxides for mitigating PM2.5 air pollution, Science 374 (2021) 758–762, https://doi.org/10.1126/science.abf8623.
[76] J. Yuan, Z. Wang, J. Liu, J. Li, J. Chen, Potential risk of NH3 slip arisen from catalytic inactive site in selective catalytic reduction of NOx with metal-free carbon catalysts, Environ. Sci. Technol. 57 (2023) 606–614, https://doi.org/10.1021/acs.est.2c06289.
[77] M.J. Illán-Gómez, E. Raymundo-Piñero, A. Garcıa-Garcıa, A. Linares-Solano, C. Salinas-Martınez de Lecea, Catalytic NOx reduction by carbon supporting metals, Appl. Catal. B Environ. 20 (1999) 267–275, https://doi.org/10.1016/S0926-3373(98)00119-2.
[78] L. Chen, S. Ren, W. Liu, J. Yang, Z. Chen, M. Wang, Q. Liu, Low-temperature NH3-SCR activity of M (M = Zr, Ni and Co) doped MnOx supported biochar catalysts, J. Environ. Chem. Eng. 9 (2021) 106504, https://doi.org/10.1016/j.jece.2021.106504.
[79] J. Yang, J. Zhou, W. Tong, T. Zhang, M. Kong, S. Ren, Low-temperature flue gas denitration with transition metal oxides supported on biomass char, J. Energy Inst. 92 (2019) 1158–1166, https://doi.org/10.1016/j.joei.2018.06.002.
[80] D. Mehandjiev, E. Bekyarova, M. Khristova, Study of Ni-impregnated active carbon, J. Colloid Interface Sci. 192 (1997) 440–446, https://doi.org/10.1006/jcis.1997.4901.
[81] A. Nzihou (Ed.), Handbook on Characterization of Biomass, Biowaste and Related by-Products, Springer International Publishing, 2020, https://doi.org/10.1007/978-3-030-35020-8.
[82] L.M.R. Millan. Steam gasification of tropical lignocellulosic agrowaste: Impact of biomass characteristics on the gaseous and solid by-products, thesis, 2018. https://theses.fr/2018EMAC0011208.
[83] A.C. Ghogia, theses.fr – Amel cydric Ghogia, Développement de catalyseurs monolithiques structurés du type Co/C/mousse pour le procédé de synthèse Fischer-Tropsch, thesis, http://www.theses.fr/s184711, 2021 (accessed October 18, 2021).
[84] M. Ducousso, Gasification Biochar Reactivity toward Methane Cracking, thesis, Ecole des Mines d'Albi-Carmaux, 2015, https://tel.archives-ouvertes.fr/tel-01411838 (accessed October 28, 2020).
[85] J. Jeon, J.H. Park, S. Wi, S. Yang, Y.S. Ok, S. Kim, Characterization of biocomposite using coconut oil impregnated biochar as latent heat storage insulation, Chemosphere 236 (2019) 124269, https://doi.org/10.1016/j.chemosphere.2019.06.239.